Theor Chem Acc (2011) 130:483–489
DOI 10.1007/s00214-011-1026-5

REGULAR ARTICLE

Tuning graphene nanoribbon field effect transistors via controlling doping level

Lu Wang · Jiaxin Zheng · Jing Zhou · Rui Qin · Hong Li · Wai-Ning Mei · Shigeru Nagase · Jing Lu

Received: 6 March 2011 / Accepted: 13 August 2011 / Published online: 30 August 2011

Abstract By performing first-principles transport simulations, we demonstrate that *n*-type transfer curves can be obtained in armchair-edged graphene nanoribbon field effect transistors by the potassium atom and cobaltocene molecule doping, or substituting the carbon by nitrogen atom. The Dirac point shifts downward from 0 to −12 V when the *n*-type impurity concentration increases from 0 to 1.37%, while the transfer curves basically maintain symmetric feature with respect to the Dirac point. In general, the on/off current ratios are decreased and subthreshold swings are increased with the increasing doping level. Therefore, the performance of armchair-edged graphene nanoribbon field effect transistors can be controlled via tuning the impurity doping level.

Keywords Graphene nanoribbon · Field effect transistor · Ab initio calculation

1 Introduction

Graphene, a single layer of graphite, possesses extraordinary electrical, thermal, and mechanical properties arising from its unique structure [1–4]. Its quasi-one-dimensional form, graphene nanoribbon (GNR) [5], is infinite in length and finite in width about <1 μm to 1 nm. They have attracted extensive interest recently because they are recognized as a new class of materials and building blocks for nanoelectronics and spintronics [6–8]. Among them, the GNR field effect transistors (GNR-FETs) have been studied theoretically and readily achieved in experiments [9–13]. Yan et al. [9] performed electron transport calculations for pristine GNR-FET with the channel width about 1.1 nm and predicted that the current–gate voltage (I–V_{gate}) characteristics are ambipolar and the Dirac point voltage, where the transition from electron to hole transport occurs, is near zero indicating that the GNR is an intrinsic semiconductor in its undoped state. Afterward, the predicted I–V_{gate} characteristics were proved experimentally for a GNR-FET with the channel width about 1 μm [10]. Furthermore, *p*-type I–V_{gate} characteristics has been observed for GNR-FETs with the channel width ranging from 50 nm down to sub-10 nm in the experimental study performed by Li et al. [11]. Moreover, Wang et al. [12] reported that the *n*-type GNR-FET can be functionalized by doping ammonia molecules to the sub-10 nm GNRs.

In the present work, we investigate, by using first-principles calculations, the effects of three kinds of doping with different doping concentrations on the transport properties of armchair-edged GNRs (AGNR): they are adsorptions of

Dedicated to Professor Shigeru Nagase on the occasion of his 65th birthday and published as part of the Nagase Festschrift Issue.

Electronic supplementary material The online version of this article (doi:10.1007/s00214-011-1026-5) contains supplementary material, which is available to authorized users.

L. Wang · J. Zheng · J. Zhou · R. Qin · H. Li · J. Lu (✉)
State Key Laboratory for Mesoscopic Physics and Department of Physics, Peking University, Beijing 100871, People's Republic of China
e-mail: jinglu@pku.edu.cn

L. Wang · S. Nagase
Department of Theoretical and Computational Molecular Science, Institute for Molecular Science, Okazaki 444-8585, Japan

L. Wang · W.-N. Mei
Department of Physics, University of Nebraska at Omaha, Omaha, NE 68182-0266, USA

potassium atoms and cobaltocene ($CoCp_2$) molecules, and the substitution of edge C atoms by N atoms. We demonstrate that the transfer characteristics of AGNR-FETs can be controlled by modifying the concentration of dopants, which would be beneficial for the design of tunable GNR-FET devices.

2 Computational details

Density functional theory (DFT) calculations are performed within periodic boundary conditions (PBC) as implemented in SIESTA code [14]. The generalized gradient approximation (GGA) of the Perdew–Burke–Ernzerhof (PBE) [15] form is used as the exchange–correlation functional. We employ the norm-conserving pseudopotentials, linear combination of atomic numerical orbitals formalism, and optimized basis sets of the double-ζ quality including polarization functions with the real-space mesh cutoff 400 Ry. The Monkhorst–Pack [16] $1 \times 1 \times 50$ k-point grid is used to sample the one-dimensional Brillouin zone. All the parameters were well tested and adopted in our previous research [17].

We choose an armchair-edged GNR (9-AGNR) with H termination as a model system to study the effects of doping. We use a uniform orthogonal $30 \times 20 \times 30.7$ Å^3 supercell for all the structures, which contains seven unit cells of 9-AGNR (Fig. 1a) together with the dopants such as the K atoms and $CoCp_2$ molecules adsorbed on the surface of 9-AGNR as displayed in Fig. 1b and c, whereas one C atom on the edge substituted by N as showed in Fig. 1d. The structures with two or three dopants are showed in Figure S1 of Supporting Information. Geometry optimization is performed for the pristine and doped 9-AGNRs until the maximum force acting on each atom is smaller than 0.01 eV/Å.

We carry out first-principles transport properties calculations by using the non-equilibrium Green's function (NEGF) formalism combined with DFT as implemented in ATK 2008.10 code [18, 19]. We employ a single-ζ basis set plus polarization with the mesh cutoff energy of 150 Ry, and the pseudopotentials and exchange–correlation functional are set to be the same as those used in the electronic property calculations. A two-probe model is constructed with a central scattering region connected to left and right electrodes. The Green's function and self-energies are calculated for the central scattering region, and the electrodes are semi-infinite metallic structures with the electronic properties calculated separately and using periodic boundary conditions. The electric current I under gate voltage V_{gate} and bias voltage V_{bias} is calculated using the Landauer–Büttiker formula [20] :

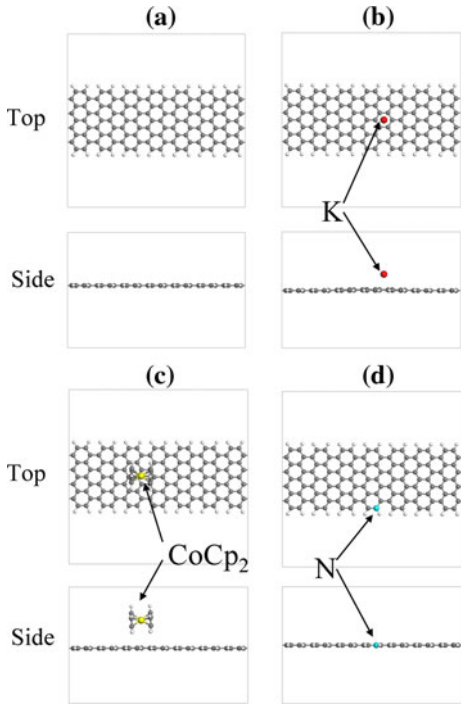

Fig. 1 Structures of the **a** pristine 9-AGNR and 9-AGNRs with **b** K atom adsorbed **c** $CoCp_2$ molecule adsorbed, and **d** one edge C atom substituted by N. *Gray*, *white*, *red*, *yellow*, and *cyan balls* are the C, H, K, Co, and N atoms, respectively

$$I(V_{\text{gate}}, V_{\text{bias}}) = \frac{2e}{h} \int_{-\infty}^{\infty} \{T(E, V_{\text{gate}}, V_{\text{bias}})[f_L(E-\mu_L) - f_R(E-\mu_R)]\} \mathrm{d}E \quad (1)$$

where $T(E,V_{\text{gate}},V_{\text{bias}})$ is the transmission probability at a given gate voltage V_{gate} and bias voltage V_{bias}, $f_{\text{L/R}}$ is the Fermi–Dirac distribution function for the left (L)/right (R) electrode, and $\mu_{\text{L}}/\mu_{\text{R}}$ is the electrochemical potential of the left (L)/right (R) electrode. A small bias voltage of 20 mV is applied for all the calculations. The role of gate electrode is to shift the scattering region part of the Hamiltonian with potential V_{gate} by assuming that the gate electrode induces an external potential localized in the scattering region.

Our AGNR-FET model (Fig. 2a) is composed of a 17.5 Å long and 11.6 Å wide pristine 9-AGNR that serves as a semiconducting channel and two metallic zigzag GNRs (6-ZGNRs) playing the roles of source and drain electrodes. Such an AGNR-FET model is similar to that proposed in the early study [9] and possesses smooth interface between the semiconducting and metallic GNRs, thus minimizing the contact resistance. More importantly, it provides large surface area and wide edges for doping and substitution. A series of electron transport calculations are performed for these

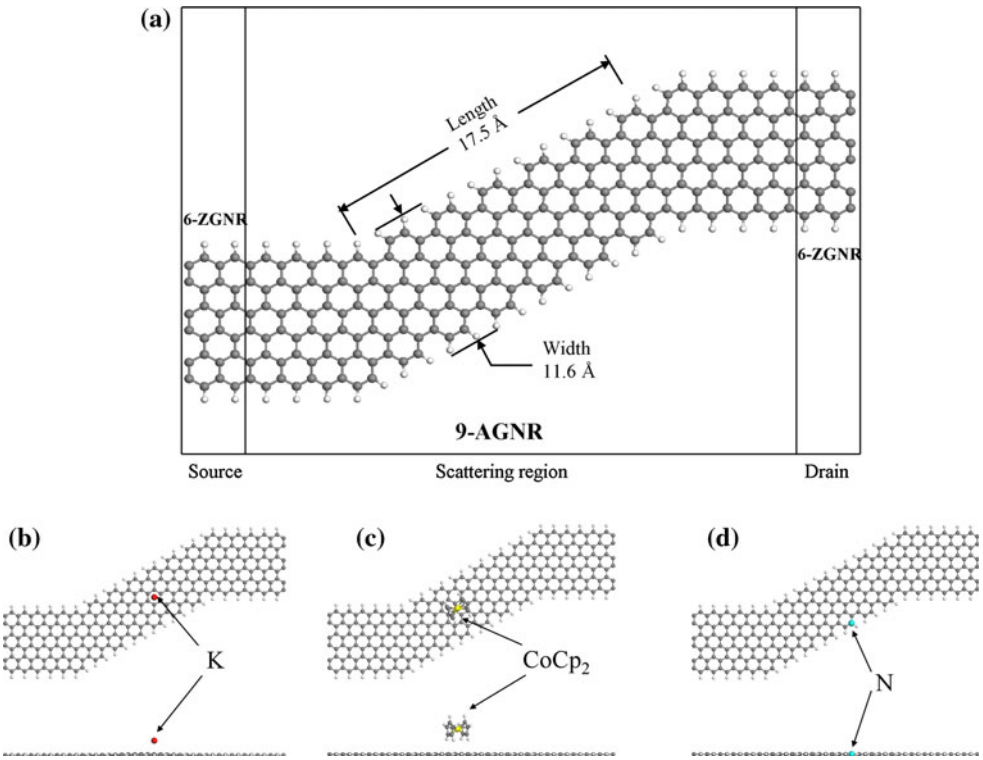

Fig. 2 **a** Undoped AGNR-FET model. AGNR-FET models with **b** one K atom **c** one $CoCp_2$ molecule adsorbed and **d** one edge C atom substituted by N. *Gray*, *white*, *red*, *yellow*, and *cyan balls* are the C, H, K, Co, and N atoms, respectively

AGNR-FET models, with both pristine and doped channels as displayed in Fig. 2 and Figure S2 of Supporting Information.

3 Results and discussion

We first verify that the pristine 9-AGNR is a semiconductor with a bandgap of 0.88 eV, which agrees well with the previous studies [5]. Then in Fig. 3 we present the band structures of the pristine and doped 9-AGNRs. The impurity bands caused by the valance electrons of K and $CoCp_2$ are denoted as α bands in Fig. 3b–d and β bands in Fig. 3e–g. The π^*-bands are occupied by electrons from dopants, and the occupation level increases with the increasing doping level. Given a doping concentration, the occupation level is higher for K and N doping than for $CoCp_2$ doping. This clearly indicates that K, $CoCp_2$, and N dopings are a *n*-type doping, and K and N are stronger electron donor than $CoCp_2$. When the doping concentration increases, we observe that the π^*-band mixes strongly with the impurity bands: such as α bands in Fig. 3c–d and β bands in Fig. 3f–g. Mulliken population analysis [21] is performed, and the results are listed in Table 1. We observe significant charge transferred from K atoms and $CoCp_2$ molecules to the 9-AGNR. The electron transfer is stronger for K than $CoCp_2$ (comparing a electron transfer of 0.99 $|e|$ per K atom with 0.70 $|e|$ per $CoCp_2$), a result consistent with the difference in the π^*-band filling.

As shown in Fig. 4, the pristine AGNR-FET is an excellent ambipolar transistor, and its I–V_{gate} (transfer) curve has nearly symmetric characteristic. This character can be explained in terms of the band structure of the pristine 9-AGNR (Fig. 3a), in which the π- and π^*-bands are nearly symmetric with respect to the Fermi level. After various doping and/or substitutions at the semiconducting channel of AGNR-FET, we observe the transfer curves shift downward from -4.5 to -12 V with the increasing doping concentration, typical of *n*-type FET. This behavior can be understood as following: In general, an increase in donor concentration leads to higher electron carrier concentration available for conduction. Hence the gate voltage should be further decreased in order to deplete all the additional electron carriers resided in AGNR-FET. Therefore, the transport properties of the AGNR-FETs can be effectively controlled by the doping concentration. The speed of downward shift with respect to the doping concentration of K and N doping is larger than that of $CoCp_2$ doping, and this difference is consistent with the higher electron-donating ability of K and N doping.

At low concentrations less than 1%, the transfer curves remain their symmetric nature with respect to the Dirac point. When the concentration is higher than 1%, the transfer curves of K- and $CoCp_2$-doped AGNR-FETs start to show somewhat asymmetric behavior, i.e., green curves in Fig. 4a and b. Again we can explain that based on the band structures of the doped GNRs in Fig. 3b–g when the impurity concentration is low, such as those in Fig. 3b and

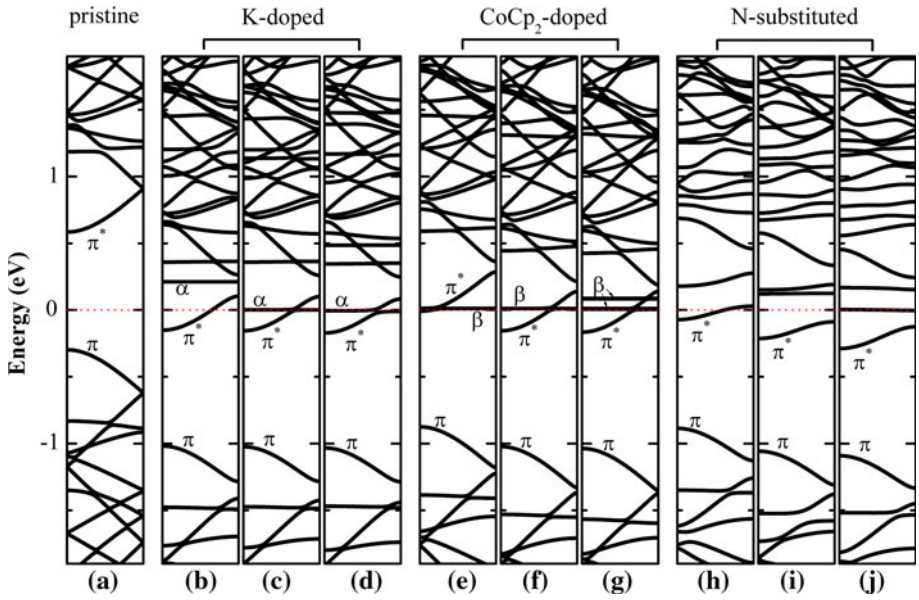

Fig. 3 Band structures of the **a** pristine 9-AGNR, and 9-AGNR with different adsorptions, from **b–d** are one to three K atoms, from **e–g** are one to three $CoCp_2$ molecules, and from **h–j** are one to three edge C atoms substituted by N. α and β indicate the impurity bands caused by K and $CoCp_2$, respectively

Table 1 Closest distances (d) between the dopants and graphene, binding energies, and charge states of the 9-AGNR with one, two, and three dopants

	d (Å)	Binding energy (eV/per dopant)	Charge (|e|)		
9-AGNR + K	2.67	0.67	−0.99[a]	−1.94[b]	−2.81[c]
9-AGNR + $CoCp_2$	3.21	1.10	−0.70[a]	−1.51[b]	−2.20[c]

Negative value of charge indicates that the dopant donates electron to the 9-AGNR

[a] One dopant; [b] two dopants; [c] three dopants

e, the π- and π^*-bands nearly maintain symmetry with respect to their midpoint; when the impurity concentration increases, we observe that the band structures show asymmetric behavior, such as those in Fig. 3e and g, due to the mixture between the π^*- and impurity bands. The symmetry of the π- and π^*-bands of N-substituted GNRs does not change significantly as shown in Fig. 3h–j; thus the transfer curves of the corresponding AGNR-FETs (Fig. 4c) nearly maintain their symmetry when the impurity concentration increases.

I_{on}/I_{off} is the key parameter for real FET devices [22, 23], where I_{on} and I_{off} are the on-state and off-state currents, respectively. The I_{on} for the pristine 9-AGNR channel is about 0.96 μA, and the minimum leakage current I_{off} is about 0.008 μA, leading to a I_{on}/I_{off} ratio of about 124. After doping, the I_{on}/I_{off} ratio, displayed in Fig. 5a, has a decrease tendency with the increasing doping level. As we noticed the current range in intrinsic and doped AGNR-FETs is of the order of μA, we expect that the calculated I_{on}/I_{off} ratios are significant for realistic nanodevices. The subthreshold swing (S) is used to determine the FET efficiency when turning on or off by changing the gate voltage and it is defined as the gate voltage required to change the current by one order of magnitude in subthreshold region. The transistors with small S are favorable for their small gate voltage variation and low power consumptions in operation. We take S as average $dV_{gate}/d(\log I)$ over the V_{gate} to the left and right side of the Dirac point and present them in Fig. 5b as a function of the impurity concentration. We notice that the calculated S generally increases with the impurity concentration from 1,200 to 3,600 mV/decade due to impurity scattering, which is about four to nine times the minimum experimental value (400 mV/decade) obtained in the organic FET made from single-walled carbon nanotube [24]. The performance of GNR-FET is generally degraded with the increasing doping level in terms of I_{on}/I_{off} ratio and subthreshold swing two criterions.

Transmission eigenchannels are the scattering states [20] with a well-defined transmission eigenvalues T_n with $0 \leq T_n \leq 1$. The individual transmission eigenvalue T_n represents the probability that the incoming wave functions are transmitted from one electrode to the other side and adds up to constitute the total transmission, $T = \Sigma_n T_n$. In our cases, the majority of the transmission is carried out in the first eigenchannel with smaller transmission eigenvalues for the other eigenchannels ($<10^{-3}$). We plot the calculated first transmission eigenchannel and the

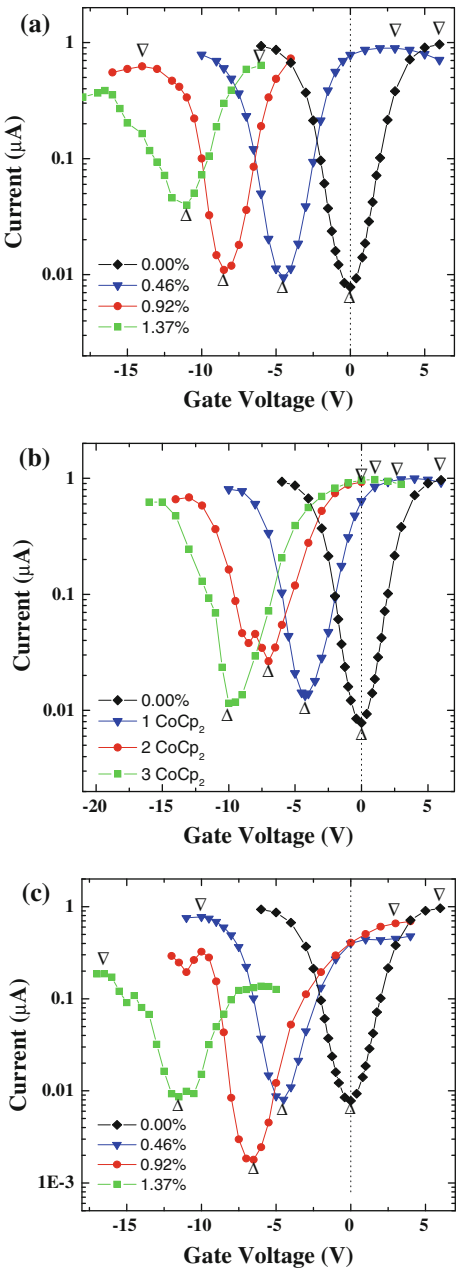

Fig. 4 I–V_{gate} characteristics of AGNR-FET with the semiconducting channel made from 9-AGNR with **a** K atoms **b** $CoCp_2$ adsorbed and **c** edge C atoms substituted by N. Δ indicates the locations of the Dirac points, generally regarded as off-states, and ∇ stands for the highest points of the I–V_{gate} *curves* are our choices as the on-states, respectively. The source-drain voltage is 20 meV

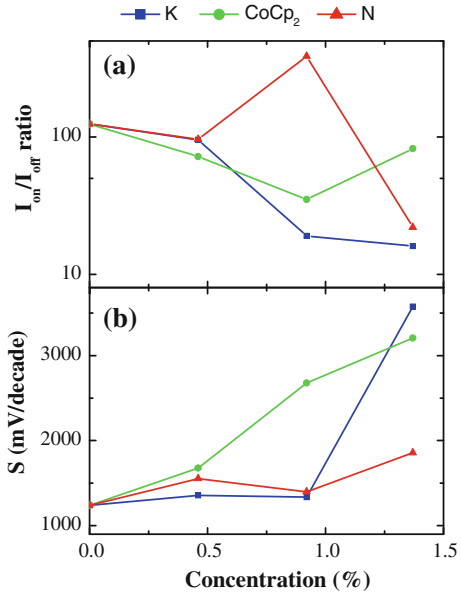

Fig. 5 **a** I_{on}/I_{off} ratios and **b** subthreshold swings of the doped AGNR-FET as a function of doping level

corresponding transmission eigenvalue (T_1) at the Fermi level for the on- and off-state of the pristine and doped AGNR-FET in Fig. 6. We note that at on-state T_1 is larger than 0.5 as shown in Fig. 6a–d, indicating that majority of the incoming wave function is capable of reaching the other electrode. By contrast, most of the incoming wave function is scattered back and not able to reach to the other electrode at off-state for their small T_1 as shown in Fig. 6e–h. Hence, we notice that the transmission eigenvalues of the on-states are one order of magnitude larger than those of the corresponding off-states, contributing to the large I_{on}/I_{off} ratios. Based on Fig. 5, we recognize that after doping the on-state T_1 is 30–50% smaller than that of pristine AGNR-FET, which we believe are caused by impurity scatterings: that is when K and $CoCp_2$ were doped, the eigenvalues dropped more than 40% suggesting that the impurity effects at the central region of GNR is more important than when N atoms substituted at the edge. Hence we anticipate that doping atom at edge is an efficient way to reduce scattering influence. At the same time, there are more residual wave functions at off-states after doping than that of pristine AGNR-FET, which we expect is also due to doping.

The present results are based on AGNRs whose moderate band gaps are suitable for achieving high-performance FETs. According to our calculations, electron doping of AGNRs induced by K and $CoCp_2$ adsorption occupies the conduction band of AGNRs approximately in a rigid band filling way while by N substitution is not a rigid band filling way. The ground states of zigzag-edged GNRs (ZGNRs) are antiferromagnetic semiconducting states with smaller band gaps. K and $CoCp_2$ adsorption on ZGNRs also lead to a rigid band filling of the conduction band by electrons. However, N substitution does not follow this filling mode. A calculation by Li et al. [25] revealed that ZGNRs can be converted into spin gapless semiconductors, nonmagnetic metals, or half-metals by N doping. Therefore, we believe that doping ZGNRs by K and $CoCp_2$

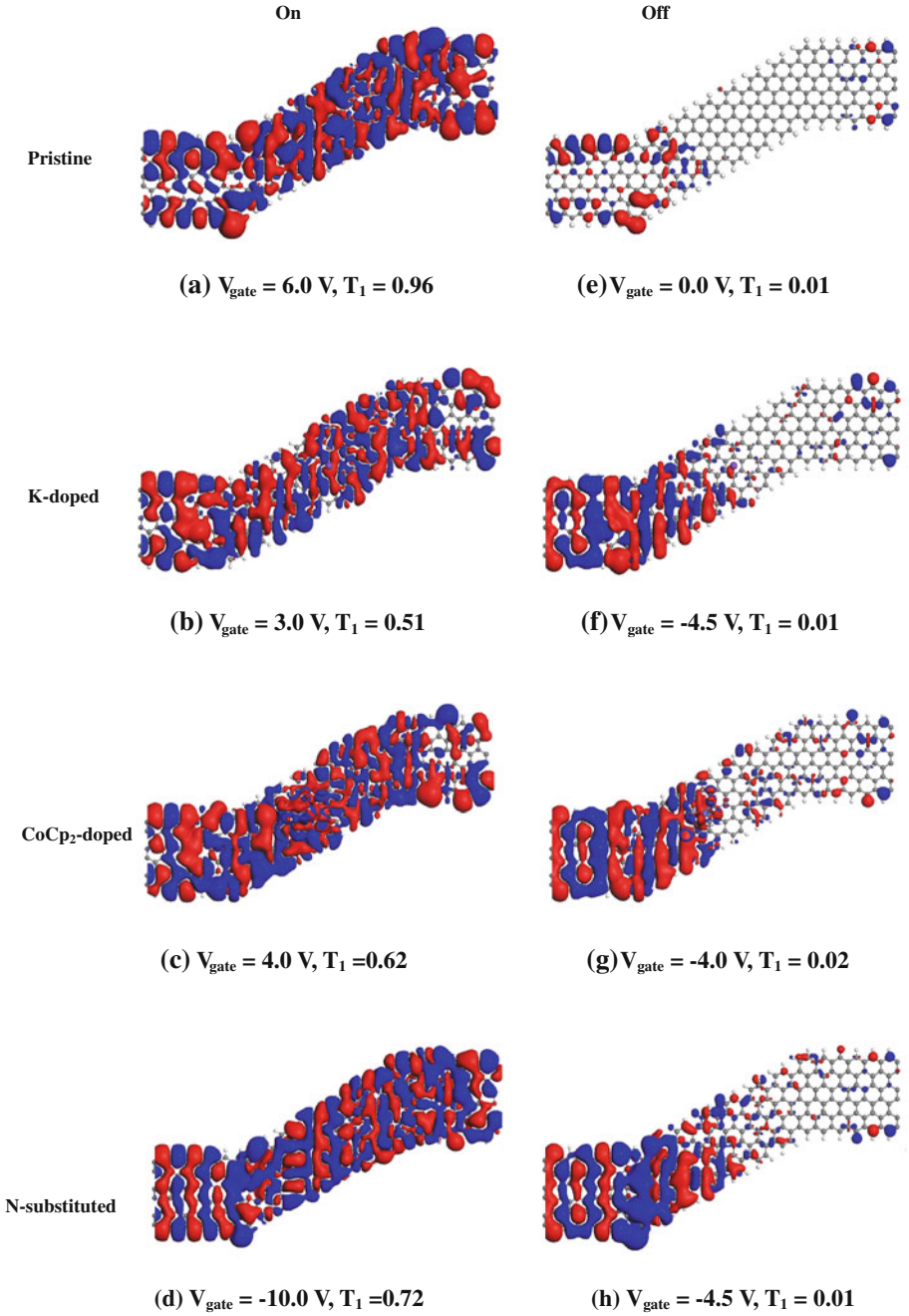

Fig. 6 First transmission eigenchannel at the Fermi level for the pristine 9-AGNR (**a**, **e**), 9-AGNR with one K atom (**b**, **f**), one $CoCp_2$ molecule adsorbed (**c**, **g**), and one edge C atom substituted by N (**d**, **h**). (**a**–**d**) and (**e**–**h**) are on- and off-states, respectively. Isovalue is chosen to be 5×10^{-3} a.u. *Red* and *blue* indicate the positive and negative regions of the wave functions, respectively. The corresponding gate voltage (V_{gate}) and calculated transmission eigenvalue T_1 are also given. **a** $V_{gate} = 6.0$ V, $T_1 = 0.96$, **b** $V_{gate} = 3.0$ V, $T_1 = 0.51$, **c** $V_{gate} = 4.0$ V, $T_1 = 0.62$, **d** $V_{gate} = -10.0$ V, $T_1 = 0.72$, **e** $V_{gate} = 0.0$ V, $T_1 = 0.01$, **f** $V_{gate} = -4.5$ V, $T_1 = 0.01$, **g** $V_{gate} = -4.0$ V, $T_1 = 0.02$, **h** $V_{gate} = -4.5$ V, $T_1 = 0.01$

adsorption can also result in adjustable *n*-type FET since the band gap between the conduction and valence bands remains but N substitution fails to achieve this goal since the band gap between the conduction and valence bands vanishes. However, *n*-type doped ZGNRs induced by K and $CoCp_2$ adsorption are unsuitable for high-performance FET because their band gaps are too small (<0.4 eV) and any successor to the silicon metal–oxide–semiconductor FET must have a large on/off ratio of between 10^4 and 10^7, which requires semiconducting channel of a FET with a sizeable band gap, preferably 0.4 eV or more [26].

4 Conclusion

In summary, we have performed extensive first-principles calculations and revealed that the semiconducting GNRs can be converted into *n*-type by adsorption of K atoms or $CoCp_2$ molecules, or substitution of edge C by N atoms. The Dirac point shift downward with the increasing impurity concentration, but the transfer curves basically maintain symmetric feature with respect to the Dirac point. The on/off ratios are generally decreased and subthreshold swings are generally increased with the increasing doping

concentration. Our results indicate that one can control the performance of GNR-FET by changing the impurity doping level.

Acknowledgments This work was supported in Japan by the Grant-in-Aid for Scientific Research on Priority Area and Next Generation Super Computing Project (Nanoscience Program) from the MEXT of Japan, in China by the NSFC (Grant Nos. 10774003, 10474123, 10434010, 90606023, and 20731160012) and National 973 Projects (Nos. 2002CB613505 and 2007CB936200, MOST of China), and in USA by Nebraska Research Initiative and DOE DE-EE0003174.

References

1. Stankovich S, Dikin DA, Dommett GHB, Kohlhaas KM, Zimney EJ, Stach EA, Piner RD, Nguyen ST, Ruoff RS (2006) Graphene-based composite materials. Nature 442(7100):282–286
2. Geim AK, Novoselov KS (2007) The rise of graphene. Nat Mater 6(3):183–191
3. Novoselov KS, Geim AK, Morozov SV, Jiang D, Zhang Y, Dubonos SV, Grigorieva IV, Firsov AA (2004) Electric field effect in atomically thin carbon films. Science 306(5696):666–669
4. Novoselov KS, Jiang D, Schedin F, Booth TJ, Khotkevich VV, Morozov SV, Geim AK (2005) Two-dimensional atomic crystals. Proc Natl Acad Sci USA 102(30):10451–10453
5. Son Y-W, Cohen ML, Louie SG (2006) Energy Gaps in Graphene Nanoribbons. Phys Rev Lett 97(21):216803
6. Son YW, Cohen ML, Louie SG (2006) Half-metallic graphene nanoribbons. Nature 444(7117):347–349
7. Barone V, Hod O, Scuseria GE (2006) Electronic structure and stability of semiconducting graphene nanoribbons. Nano Lett 6(12):2748–2754
8. Han MY, Ozyilmaz B, Zhang YB, Kim P (2007) Energy band-gap engineering of graphene nanoribbons. Phys Rev Lett 98(20):206805
9. Yan QM, Huang B, Yu J, Zheng FW, Zang J, Wu J, Gu BL, Liu F, Duan WH (2007) Intrinsic current-voltage characteristics of graphene nanoribbon transistors and effect of edge doping. Nano Lett 7(6):1469–1473
10. Schedin F, Geim AK, Morozov SV, Hill EW, Blake P, Katsnelson MI, Novoselov KS (2007) Detection of individual gas molecules adsorbed on graphene. Nat Mater 6(9):652–655
11. Li XL, Wang XR, Zhang L, Lee SW, Dai HJ (2008) Chemically derived, ultrasmooth graphene nanoribbon semiconductors. Science 319(5867):1229–1232
12. Wang XR, Li XL, Zhang L, Yoon Y, Weber PK, Wang HL, Guo J, Dai HJ (2009) N-Doping of Graphene Through Electrothermal Reactions with Ammonia. Science 324(5928):768–771
13. Wang ZF, Li QX, Shi QW, Wang XP, Hou JG, Zheng HX, Chen J (2008) Ballistic rectification in a Z-shaped graphene nanoribbon junction. Appl Phys Lett 92(13):3
14. Soler JM, Artacho E, Gale JD, Garcia A, Junquera J, Ordejon P, Sanchez-Portal D (2002) The SIESTA method for ab initio order-N materials simulation. J Phys: Condens Mat 14(11):2745–2779
15. Perdew JP, Burke K, Ernzerhof M (1996) Generalized gradient approximation made simple. Phys Rev Lett 77(18):3865–3868
16. Monkhorst HJ, Pack JD (1976) Special points for Brillouin-zone integrations. Phys Rev B 13(12):5188
17. Wang L, Cai ZX, Wang JY, Lu J, Luo GF, Lai L, Zhou J, Qin R, Gao ZX, Yu DP, Li GP, Mei WN, Sanvito S (2008) Novel One-Dimensional Organometallic Half Metals: Vanadium-Cyclopentadienyl, Vanadium-Cyclopentadienyl-Benzene, and Vanadium-Anthracene Wires. Nano Lett 8(11):3640–3644
18. Taylor J, Guo H, Wang J (2001) Ab initio modeling of quantum transport properties of molecular electronic devices. Phys Rev B 63(24):245407
19. Brandbyge M, Mozos JL, Ordejon P, Taylor J, Stokbro K (2002) Density-functional method for nonequilibrium electron transport. Phys Rev B 65(16):165401
20. Datta S (1995) Electronic Transport in Mesoscopic Systems. Cambridge University Press, Cambridge, England
21. Mulliken RS (1955) Electronic Population Analysis on Lcao-Mo Molecular Wave Functions.3. Effects of Hybridization on Overlap and Gross Ao Populations. J Chem Phys 23(12):2338–2342
22. Newman CR, Frisbie CD, da Silva DA, Bredas JL, Ewbank PC, Mann KR (2004) Introduction to organic thin film transistors and design of n-channel organic semiconductors. Chem Mat 16(23): 4436–4451
23. Xia FN, Farmer DB, Lin YM, Avouris P (2010) Graphene Field-Effect Transistors with High On/Off Current Ratio and Large Transport Band Gap at Room Temperature. Nano Lett 10(2):715–718
24. Qi P, Javey A, Rolandi M, Wang Q, Yenilmez E, Dai H (2004) Miniature Organic Transistors with Carbon Nanotubes as Quasi-One-Dimensional Electrodes. J Am Chem Soc 126(38):11774–11775
25. Li Y, Zhou Z, Shen P, Chen Z (2009) Spin Gapless Semiconductor-Metal-Half-Metal Properties in Nitrogen-Doped Zigzag Graphene Nanoribbons. ACS Nano 3(7):1952–1958
26. Schwierz F (2010) Graphene Transistors. Nat Nanotechnol 5(7): 487–496